Available online at www.sciencedirect.com
ScienceDirect
Journal of Molecular Catalysis A: Chemical 262 (2007) 149–155
JOURNAL OF MOLECULAR CATALYSIS A: CHEMICAL
www.elsevier.com/locate/molcata

Microwave radiation solid-phase synthesis of phosphotungstate nanoparticle catalysts and photocatalytic degradation of formaldehyde

Qian Deng [a], Wenhui Zhou [a], Xiaomei Li [a], Zhenshan Peng [a], Shaoliang Jiang [b], Ming Yue [a], Tiejun Cai [a,*]

[a] *College of Chemistry & Chemical Engineeing, Hunan University of Science & Technology, Xiangtan 411201, PR China*
[b] *Institute of New Catalytic Material Science, College of Chemistry, Nankai University, Tianjin 300071, PR China*

Available online 23 August 2006

Abstract

Photocatalysts $M_3PW_{12}O_{40}$ ($M = NH_4^+$, Cs^+, Ag^+, Cu^{2+}) were prepared by microwave radiation solid-phase synthesis method. The results from SEM and XRD characterization reveal that the average particle size of $M_3PW_{12}O_{40}$ is 15–80 nm. Diffuse reflectance UV–vis spectra of $M_3PW_{12}O_{40}$ shows that the absorption band shifted from 260 to 270–350 nm and become broad in comparison with those of $H_3PW_{12}O_{40}$. The results of photocatalytic degradation of formaldehyde prove that the shift of UV–vis absorption band is proportionally related to the activity of the catalyst. The $Cu_3(PW_{12}O_{40})_2$ catalyst which has the maximal red shift to 350 nm of its UV–vis absorption band is found to be the most efficient catalyst. When the concentration of formaldehyde is 32.79 mg m^{-3}, the conversion of the formaldehyde is basically completed under the flow rate of 40 ml min^{-1} over 0.1 g $M_3PW_{12}O_{40}$ catalyst. The $M_3PW_{12}O_{40}$ catalysts prepared by this method are stable and the regeneration of the catalysts is easy. The catalysts have promising applications in the photocatalytic degradation of organic contamination.
© 2006 Elsevier B.V. All rights reserved.

Keywords: Phosphotungstate; Photocatalyst; Nanoparticle; Microwave; Solid-state synthesis

1. Introduction

As our living standard is rapidly improving and the pace of industrialization is accelerating, the environmental pollution is becoming a serious problem. The photocatalytic degeneration of organic contamination is one of the effective ways to eliminate environment pollutant. At present, the research of this topic is mainly concentrated on the titanium dioxide (TiO_2) and polyoxometalates (POM) catalysts [1–11].

POM has excellent photochemical nature, and is being explored in the environmental protection domain. Among them, the photocatalytic activity of tungstate system is quite prominent. For example, some aromatic derivatives and chlorinated acetic can be photolytic mineralized with near visible or UV light in the presence of PW_{12} or SiW_{12}. These catalysts are, at least, as effective as the titanium dioxide [12–14]; The PW_{12}/TiO_2 catalyst can degrade many kinds of aqueous dye [15–20]. The activity dramatically increases when the particle size of the catalysts is in the range of nanometer [21]. Nanosize and bimodal porous polyoxotungstate–anatase can photocatalytically decomposed the organophosphorus pesticide with visible-light excitation [22]. The addition of phosphotungstate in PVC membrane induces photocatalytic degeneration of plastic membrane, which provides an effective way to eliminate white pollution [23].

The outstanding photocatalytic, electrical, magnetic properties of nano-materials and their increasing applications in many fields are drawing much attention to their preparation method. You [24] was the first who prepared polyoxometalates by room-temperature solid-phase synthesis. Its procedure is simple and can easily be repeated. However, it takes much time to grind the reactant and consumes large amount of organic solvents to eliminate the soluble reactant in the last step.

The microwave technique has its unique merit as the chemical reaction heat source [25]. First, microwave has strong penetrating power and the reaction temperature can be increased fast and evenly. Second, only the polarized material can absorb the microwave. Third, it is a "non-thermal reaction" between the microwave and the chemicals. As a result, it reduces the reaction temperature. The microwave radiation solid phase synthesis has many advantages such as rapid reaction, minimized subsequent handling, wide ranges of application, high production rate, and so on. The studies mentioned above are mostly aimed at reduc-

* Corresponding author. Tel.: +86 732 8291 350; fax: +86 732 8290 017.
E-mail address: tjcai53@163.com (T. Cai).

1381-1169/$ – see front matter © 2006 Elsevier B.V. All rights reserved.
doi:10.1016/j.molcata.2006.08.043

ing organic pollutant in liquid phase nowadays. The application of POM catalysts for the degeneration of gas phase pollutant is still limiting.

Indoor air pollution seriously harms the human health and has caused strong concerns. Among many indoor pollutants, formaldehyde is one of the major culprits. Formaldehydes introduced in home remodelling materials and processes have become huge health hazard, and are becoming an important topic of environment management.

In our study, phosphotungstate nanoparticle photocatalysts were prepared by the microwave radiation solid phase synthesis and photocatalytic performance of the catalysts was studied using simulated polluted air containing formaldehyde and methyl alcohol. The correlations between the surface property or the reaction conditions and the activity of photocatalytic catalysts were investigated for the purpose of searching a photocatalytic method of formaldehyde management.

2. Experimental

2.1. Catalysts preparation

The $(NH_4)_3PW_{12}O_{40}$ catalyst was prepared by first mixing $H_3PW_{12}O_{40}\cdot 19H_2O$ and $(NH_4)_2C_2O_4\cdot 2H_2O$ in molar ratio under grinding in carnelian mortar for 5 min, powder turned into dope. Then it was ground for 10 more minutes. The mixture was then placed into porcelain crucible and treated in the microwave oven for 5 min, with gases spillage immediately. Finally, the product not purified was calcined in air for 2 h at 250 °C, which is $(NH_4)_3PW_{12}O_{40}$ photocatalyst.

The preparation of $Cs_3PW_{12}O_{40}$, $Ag_3PW_{12}O_{40}$ and $Cu_3(PW_{12}O_{40})_2$ catalysts: $H_3PW_{12}O_{40}\cdot 19H_2O$ and $H_2C_2O_4\cdot 2H_2O$ were mixed by molar ratio (2:3) under grinding in carnelian mortar for 5 min. Then, the same molar Cs_2CO_3, $AgNO_3$ and $CuSO_4\cdot 5H_2O$ were added respectively into mortar, and continued grinding for 10 min. Then the next treatment was the same as that for $(NH_4)_3PW_{12}O_{40}$ catalyst.

The reactions were shown as follow:

$$H_3PW_{12}O_{40}\cdot 19H_2O + (NH_4)_2C_2O_4\cdot 2H_2O + O_2 \rightarrow (NH_4)_3PW_{12}O_{40}\cdot yH_2O + H_2O\uparrow + CO_2\uparrow$$

$$H_3PW_{12}O_{40}\cdot 19H_2O + Cs_2CO_3 \rightarrow Cs_3PW_{12}O_{40}\cdot yH_2O + H_2O\uparrow + CO_2\uparrow$$

$$H_3PW_{12}O_{40}\cdot 19H_2O + AgNO_3 \rightarrow Ag_3PW_{12}O_{40}\cdot yH_2O + H_2O\uparrow + NO_2\uparrow + O_2\uparrow$$

$$H_3PW_{12}O_{40}\cdot 19H_2O + CuSO_4\cdot 5H_2O \rightarrow Cu_3(PW_{12}O_{40})_2\cdot yH_2O + H_2O\uparrow + SO_3\uparrow$$

2.2. Catalytic reaction

The photocatalytic activity tests were performed in a intermission (Fig. 1a) and continuous-flow (Fig. 1b) fix-bed photoreaction system, respectively. 0.1 g catalysts were spread on the bottom of the quartz reactor (φ/8 mm; L/300 mm). The quartz reactor was in a constant temperature box irradiated under the 18 W UV lamp ($\lambda = 253.7$ nm). Atmospheric pressure air stream was bubbled in a vessel filled with formaldehyde aqua (AR reagent, containing formaldehyde 37–40% and methyl alcohol 18–20%) at a flow rate of 40 ml min^{-1}. The UV lamp was not turned on until the concentration of the feed gas was stable. The gas mixture passed through the catalyst bed equipped with a six-port valve. The products were detected by gas chromatography (GC) analysis (the CO_2 is detected using the saturated lime aqua).

2.3. Life and regeneration tests

The life test was performed in continuous-flow fix-bed photoreaction system (Fig. 1b) under the condition as shown in Section 2.2. The concentration of organic compounds was measured every 30–60 min. After 72 h of life test the activity of photocatalysts was still stable.

After photocatalytic reaction, the color of the catalysts changed into the blue except $Ag_3PW_{12}O_{40}$ that change into the black. Passing the air over the catalyst bed after the life test, the color of the catalysts was restored basically (the $Ag_3PW_{12}O_{40}$ is a grey color, which may have a few of Ag). The reactivity of catalysts was recovered by regeneration in air. It is shown that

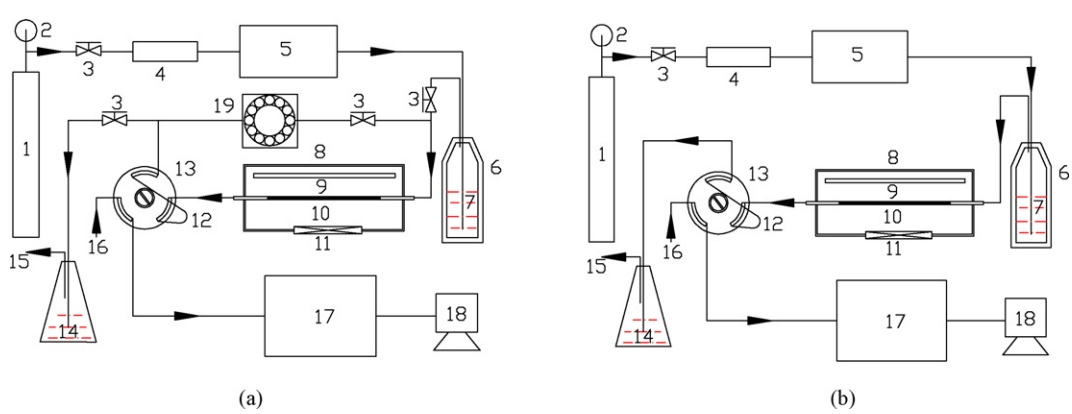

Fig. 1. Gas–solid photoreactor system: (a) intermission reactor and (b) continuous-flow reactor. (1) Air, (2) manometer, (3) valve, (4) desiccator, (5) mass flowmeter, (6) the air occurrence machine, (7) formaldehyde aqua, (8) photo-catalytic reactor, (9) UV lamp, (10) quartz reactor, (11) fan, (12) fixed amount tube, (13) six-port valve, (14) tail gas absorb, (15) put empty, (16) carring gas, (17) gas chromatography, (18) GC work station, and (19) constant flow pump.

the activity of photocatalysts is stable and the regeneration of the catalysts is easy.

2.4. Catalyst characterization

IR spectra of the catalysts were taken on a Perkin-Elmer 2000 FT-IR spectrometer by KBr tablet method in the range 4000–450 cm^{-1}. Diffuse reflectance UV–vis spectra (UV/DRS) of the solids were recorded at room temperature on a Perkin-Elmer Lambda35 UV spectrometer equipped with an integrating sphere and using $BaSO_4$ as reference. The range of scanning wavelength is 355–220 nm. The BET measurements were carried out on a Chembet-3000 BET adsorption instrument under an atmosphere of mixed H_2–N_2 containing 15% H_2 (v/v) with a temperature increasing rate of 10 °C min^{-1} and the final temperature of 700 °C. The samples were pretreated at 250 °C under Ar atmosphere for 30 min. The surface structure of the catalysts was studied by scanning electron microscopy (SEM) on a FEI Sirion200 microscope. X-ray diffraction (XRD) patterns were measured by a MSAL XD-2 powder X-ray diffractometer using Cu Kα radiation (λ = 1.54056 Å). The 2θ angles were scanned from 5° to 70°at a rate of 4° min^{-1}.

The TG-DTA curve of the catalysts was obtained on a WCT-IA differential thermal balance with a heating rate of 10 °C min^{-1}. The final temperature was 570 °C.

3. Results and discussion

3.1. Preparation of catalysts

In the preparation process of catalysts, $H_2C_2O_4{\cdot}2H_2O$ was acted as a superficial dispersant and chelator of $H_3PW_{12}O_{40}{\cdot}29H_2O$. As a result, the superficial energy of $H_3PW_{12}O_{40}{\cdot}29H_2O$ was restrained and it prevented sintering of the particles. In addition, the crystal water in the reactants created countless puny "pond", which controlled the particle size effectively [26]. $(NH_4)_2C_2O_4{\cdot}2H_2O$, Cs_2CO_3, $AgNO_3$ and $CuSO_4{\cdot}5H_2O$ could dissolve into the crystal water as M^+ and acid radical anion. In the effect of electromagnetic field of microwave and the "pseudo-liquid" phase [27] of $[PW_{12}O_{40}]^{3-}$, M^+ or M^{2+} diffused into $[PW_{12}O_{40}]^{3-}$ and formed the $M_3PW_{12}O_{40}{\cdot}yH_2O$ [28].

Because of the restricting "pond" size, the particle size of $M_3PW_{12}O_{40}$ is controlled. The microwave's strong penetrating power allows heating the sample inside-out at the same time quickly and evenly, thus the reactants H_2O, NO_2, $SO_3$and CO_2 are vaporized out instantaneously. The slipstream prevents the agglomeration of particles, forming nanoparticles of $M_3PW_{12}O_{40}$.

3.2. Characterization of the catalysts

The catalysts were characterized by FT-IR, UV/DRS and TG-DTA, SEM and XRD, and their results are shown in Figs. 2–6 and Tables 1 and 2.

FT-IR spectrum of $H_3PW_{12}O_{40}$ is shown in Fig. 2a, where the catalyst has four strong absorption peaks between 700 and 1100 cm^{-1},which are attributed to $[PW_{12}O_{40}]^{3-}$ of the Keggin structure (Table 1) [29]. The bend vibration of H–O–H bond and symmetry and dissymmetry flex vibration of O–H bond in crystal water are marked by the very strong absorption peaks at 3434.81 and 1615.30 cm^{-1}.

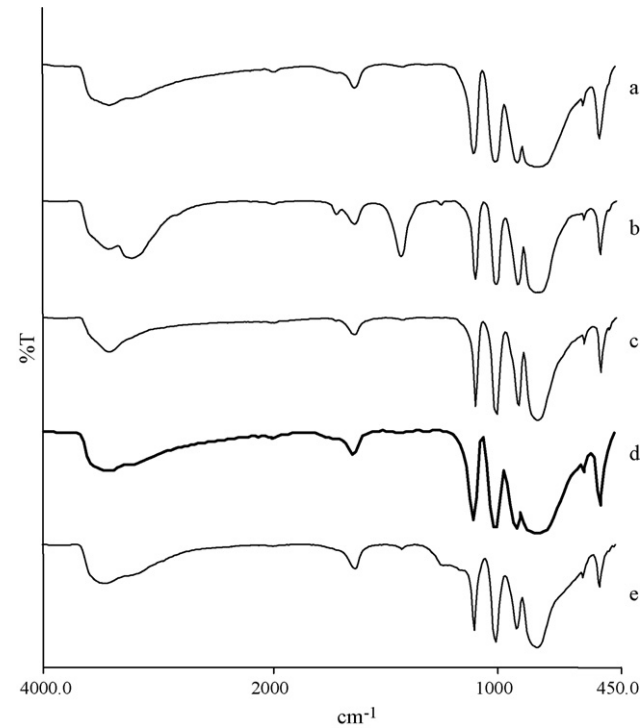

Fig. 2. FT-IR spectra of (a) $H_3PW_{12}O_{40}$, (b) $(NH_4)_3PW_{12}O_{40}$, (c) $Cs_3PW_{12}O_{40}$, (d) $Ag_3PW_{12}O_{40}$, and (e) $Cu_3(PW_{12}O_{40})_2$.

Fig. 2b–e show that the $M_3PW_{12}O_{40}$ ($M^+ = NH_4^+$, Cs^+, Ag^+, Cu^{2+}) retain the Keggin structure [29]. The four characteristic absorption peaks display blue or red shift after M^+ replaces H^+. It suggests that the chemical bond in the $[PW_{12}O_{40}]^{3-}$ is affected by the M^+, which strengthen or weaken in different degree. The very strong absorption peaks at 3434.81 and 1615.30 cm^{-1} are marked the bend vibration of H–O–H bond and symmetry

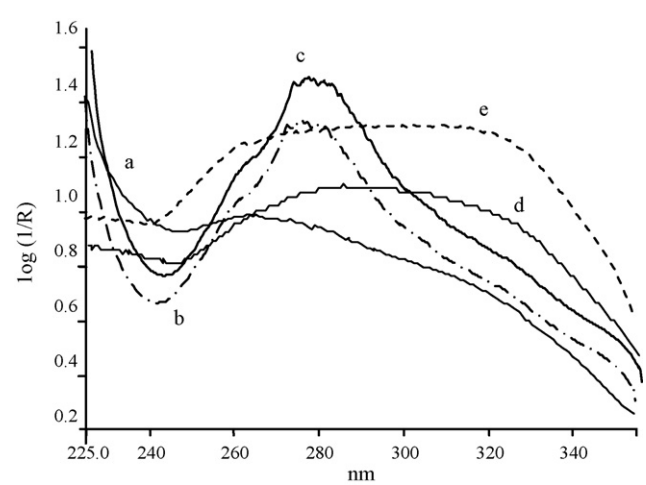

Fig. 3. Diffuse reflectance UV–vis spectra of (a) $H_3PW_{12}O_{40}$, (b) $(NH_4)_3PW_{12}O_{40}$, (c) $Cs_3PW_{12}O_{40}$, (d) $Ag_3PW_{12}O_{40}$, and (e) $Cu_3(PW_{12}O_{40})_2$.

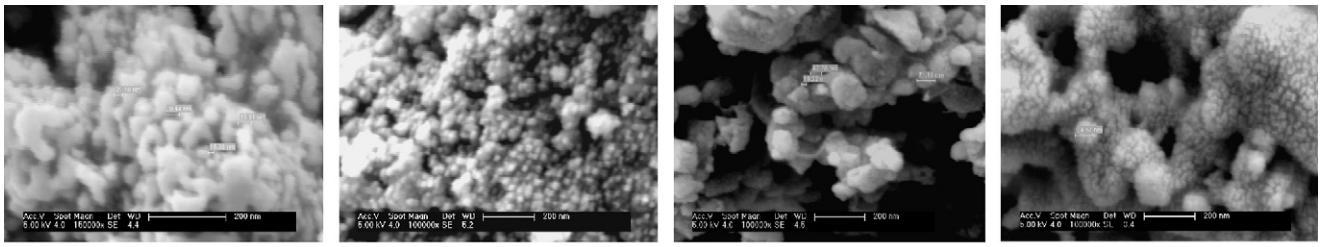

(a) (b) (c) (d)

Fig. 4. SEM spectra of (a) $(NH_4)_3PW_{12}O_{40}$, (b) $Cs_3PW_{12}O_{40}$, (c)$Ag_3PW_{12}O_{40}$, and(d) $Cu_3(PW_{12}O_{40})_2$.

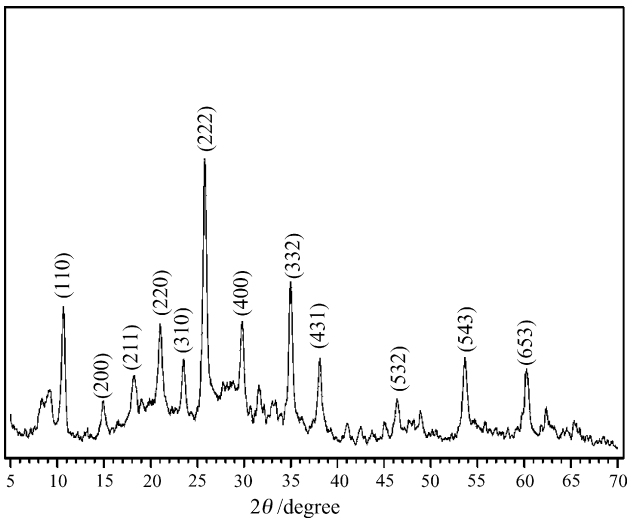

Fig. 5. XRD spectrum of $Cu_3(PW_{12}O_{40})_2$.

and dissymmetry flex vibration of O–H bond in crystal water. This indicates that there is some crystal water in $M_3PW_{12}O_{40}$ nanoparticles.

The diffuse reflectance UV–vis spectra of $M_3PW_{12}O_{40}$ ($M = NH_4^+$, Cs^+, Ag^+, Cu^{2+}) and $H_3PW_{12}O_{40}$ catalysts are presented in Fig. 3. The spectrum of $H_3PW_{12}O_{40}$ presents an intense absorption band with a maximum at 260 nm, corresponding to the charge transfer (CT) from O_{2p} to W_{5d} occurred at W–O–W bonds, which has been described as the characteristic band of Keggin-type $H_3PW_{12}O_{40}$ [30]. This band shifts from 260 to 270–350 nm and has been widened and strengthened obviously after the H^+ has been replaced by M^{n+}.

Among $M_3PW_{12}O_{40}$ ($M = NH_4^+$, Cs^+, Ag^+, Cu^{2+}), substitution of H^+ with M^{n+} benefits the electron-transfer from the $PW_{12}O_{40}^{3+}$ to cation, due to their larger size than H^+. The induction effect is advantage for the electron-transfer from $PW_{12}O_{40}^{3-}$ to M^{n+}, resulting in a lower density of electron cloud for W,O_b,O_c,O_d. Thus, bond length of W–O_c W–O_b increases and the LUMO energy decreases [27]. The lower charge transfer energy barrie from the HOMO → LUMO could be expected, so

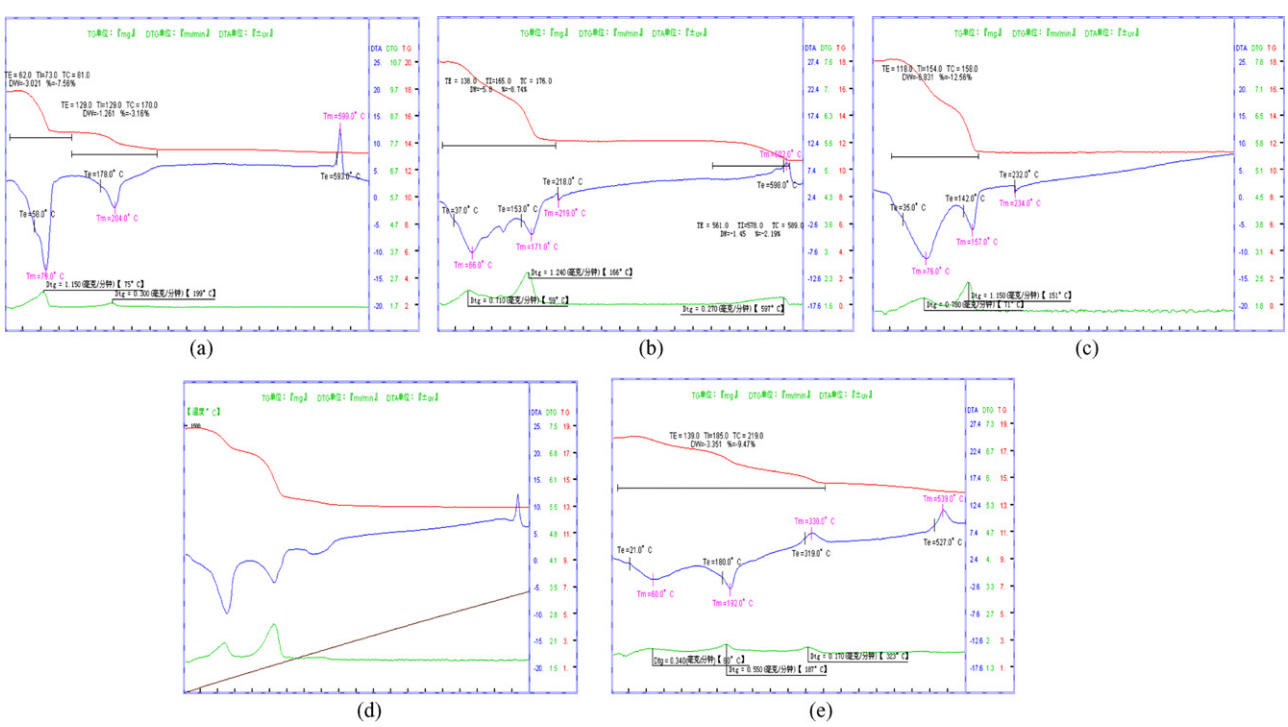

(a) (b) (c) (d) (e)

Fig. 6. TG-DTA spectra of (a) $H_3PW_{12}O_{40}$, (b) $(NH_4)_3PW_{12}O_{40}$, (c) $Cs_3PW_{12}O_{40}$, (d) $Ag_3PW_{12}O_{40}$, and (e) $Cu_3(PW_{12}O_{40})_2$.

Table 1
The FT-IR fingerprint data of Keggin structure $H_3PW_{12}O_{40}$ and phosphotungstate

Catalysts	P–O_a–W (cm^{-1})	W=O_d (cm^{-1})	W–O_b–W (cm^{-1})	W–O_c–W (cm^{-1})
$H_3PW_{12}O_{40}$	1086.57	987.47	887.96	811.67
$(NH_4)_3PW_{12}O_{40}$	1080.35	987.29	890.92	821.01
$Cs_3PW_{12}O_{40}$	1079.51	985.36	889.58	803.59
$Ag_3PW_{12}O_{40}$	1061.51	979.10	887.62	797.12
$Cu_3(PW_{12}O_{40})_2$	1080.76	983.01	891.08	800.29

that light absorption strengthened. The influence decreases as $Cu^{2+} \rightarrow Ag^+ \rightarrow Cs^+ \rightarrow NH_4^+$. The significant influence of Ag^+ and Cu^{2+} may also relates to their stronger oxidation ability after the combination with $PW_{12}O_{40}^{3-}$. The electron transfer $O \rightarrow M^{n+}$ is still produced, which has longer wave-length than that of the characteristic band [27]. Because the $O \rightarrow M^{n+}$ and $O \rightarrow W$ band overlaps so that the UV–vis absorption band is broadened. Fig. 3 shows that there is a red shift of the main peak and strengthened absorption corresponding to spectrum b (NH_4^+ salt) and spectrum c (Cs^+ salt), whereas, spectrum d (Ag^+ salt) and spectrum e (Cu^{2+} salt) become a strong broad peak.

It indicated that $M_3PW_{12}O_{40}$ catalysts increase the optical absorption and broaden the range of wavelength. The optical response of nanoparticle of $M_3PW_{12}O_{40}$ catalysts expands into near visible light region. This is in favor of the formation of charge stream and increases the utilization of light energy.

The SEM patterns for the $M_3PW_{12}O_{40}$ ($M = NH_4^+, Cs^+, Ag^+, Cu^{2+}$) catalysts are shown in Fig. 4. The SEM pattern shows that the $M_3PW_{12}O_{40}$ catalyst is in a form of anomaly spherical particles and shows some extent of agglomeration. There are some defect sites on the edge and corner site, in which the valence bond is unsaturated and has the surplus valence bond power. These defect sites usually act as adsorptive and catalytic sites. The average particle size of $(NH_4)_3PW_{12}O_{40}$, $Cs_3PW_{12}O_{40}$, $Ag_3PW_{12}O_{40}$ and $Cu_3(PW_{12}O_{40})_2$ is 40, 15, 40 and 80 nm, respectively.

The $Cs_3PW_{12}O_{40}$ (Fig. 4b) catalyst is in a form of spheroid grain, and its size is small and uniform. The average particle size of $Cs_3PW_{12}O_{40}$ is about 15 nm. The BET surface area is 213.5 $m^2\,g^{-1}$. The particle shows a tendency to agglomerate to lower the surface energy.

The particle size of the $Ag_3PW_{12}O_{40}$ (Fig. 4c) catalyst is smaller, and the average size is about 40 nm. It has larger BET surface area (179.7 $m^2\,g^{-1}$).

The $Cu_3(PW_{12}O_{40})_2$ (Fig. 4d) catalyst is in a form of tiny spheroid grain, and the average size is about 80 nm. The surface tension of $Cu_3(PW_{12}O_{40})_2$ particles is great, so agglomeration phenomenon of the catalyst grain is severe, bringing on its BET surface area is the least (70.3 $m^2\,g^{-1}$). This phenomenon makes the catalyst to form the network structure with tiny bore features, which was confirmed by the TG-DTA (Fig. 6e).

Table 2
BET surface areas ($m^2\,g^{-1}$) of $M_3PW_{12}O_{40}$ ($M = NH_4^+, Cs^+, Ag^+, Cu^{2+}$) after calcined at different temperatures

	Temperature (°C)				
	200	250	300	350	400
$(NH_4)_3PW_{12}O_{40}$	90.5	134.8	70.7	47.6	39.5
$Cs_3PW_{12}O_{40}$	127.3	213.5	131.9	79.8	42.9
$Ag_3PW_{12}O_{40}$	48.3	179.6	83.2	49.2	37.2
$Cu_3(PW_{12}O_{40})_2$	51.8	70.3	43.8	30.9	24.2

The BET surface area of the $H_3PW_{12}O_{40}$ is very small (2.4 $m^2\,g^{-1}$) originally. But after forming salt, the BET surface areas of the $M_3PW_{12}O_{40}$ increase consumedly, causing the catalyst activity sites to enlarge. The BET surface areas of the catalysts are related with the calcined temperature showing in Table 2.

When the catalysts were calcined at 250 °C, the BET surface areas of the catalysts reach maximum value. The areas decrease rapidly when the calcined temperature increases. According to thermodynamics, the nanoparticle is one kind of quasi-steady structure, so one unit volume average free energy elevates when the particle size reduces, which reduces its thermal stability. The crystal particle growth process may be considered as the smaller particle migrates to the bigger one, then the bigger particle enwraps the smaller one. This process needs to overcome the interfacial energy, which is as the activating energy. We assumed that the catalyst obtains the energy to overcome the interfacial energy at about 250 °C. When the temperature increases, the particles agglomerate and its surface area is rapidly reduced, so the catalytic active sites are reduced. This phenomenon indicates that the activity of photocatalyst is dependent on its surface area in certain degree. For same catalyst, the photocatalytic activity is related with its surface area obviouslly, which is proved by the catalytic activity of degradation of formaldehyde.

The XRD spectrum of $Cu_3(PW_{12}O_{40})_2$ is shown in Fig. 5. The crystallinity of the $Cu_3(PW_{12}O_{40})_2$ is very good. According to Scherrer's equation ($D = 0.89\lambda/\beta\cos\theta$), the particle size calculated is about 76 nm, which is in accordance with the SEM result above.

The TG-DTA curves of $H_3PW_{12}O_{40}$ catalyst are shown in Fig. 6a. An endothermic peak at $T < 130$ °C accompanying largest weight loss shows the existence of free lattice water and adsorbed water. Another endothermic peak at 130–300 °C accompanying weight loss is the emergence of a combined state lattice water which is most likely the hydrated proton. The exothermic peak at 599 °C without weight loss indicates that the catalyst is decomposed.

The TG-DTA patterns of $M_3PW_{12}O_{40}$ exhibit two to three endothermic peaks at 60–235 °C corresponding the desorption of absorbed water and lattice water (Fig. 6b–e). Except for the $Cs_3PW_{12}O_{40}$ catalyst, there is a keen-edged exothermic peak at above 527 °C without weight loss but for the decomposition

Table 3
The photocatalytic activities of catalysts to the formaldehyde degradation

Catalysts	Conversion (%)			
	69.82 mg m^{-3}	32.79 mg m^{-3}	14.85 mg m^{-3}	5.347 mg m^{-3}
$(NH_4)_3PW_{12}O_{40}$	18.32	∼100		100
$Cs_3PW_{12}O_{40}$	24.63	∼100	100	
$Ag_3PW_{12}O_{40}$	25.16	∼100	100	
$Cu_3(PW_{12}O_{40})_2$	39.36	∼100	100	

The values 69.82, 32.79, 14.85, 5.347 mg m^{-3} denotes the formaldehyde concentration.

of NH_4^+ (Fig. 6b) on the patterns of all other catalysts, which is the decomposition temperature of the $M_3PW_{12}O_{40}$ catalyst. The decomposition temperature of the $Cs_3PW_{12}O_{40}$ catalyst is above 650 °C.

On the TG-DTA of $Cu_3(PW_{12}O_{40})_2$ (Fig. 6d), a small exotherm appears after 300 °C because the growing size of the catalyst grains causes the surface energy to release. At about 330 °C, because of the breakage of the tiny bore structure, the catalyst releases a great deal of surface energy, showing an exothermic peak on the DTA curve. It confirms the result of SEM.

3.3. Catalytic activity for formaldehyde degradation

The photocatalytic formaldehyde degradation reaction was carried out in a intermission fix-bed photoreaction system (Fig. 1a) first. It is found that the activities of the catalysts that are calcinated at 250 °C for 2 h are the best, agreeing with the BET results. The catalytic activity for formaldehyde degradation is evaluated under this condition in a continuous-flow fix-bed photoreaction system (Fig. 1b). The results of the catalytic activity of the photocatalysts are shown in Table 3.

No changes of concentration and the composition of feed gas are found without the ultraviolet illumination over $(NH_4)_3PW_{12}O_{40}$, $Cs_3PW_{12}O_{40}$ and $Ag_3PW_{12}O_{40}$ catalyst, respectively. However, the composition of the feed gas obviously changes under indoor nature light rays over the $Cu_3(PW_{12}O_{40})_2$. There are a small peak of formic acid on the curve of GC and the concentration of formaldehyde is decreased, which indicates that the $Cu_3(PW_{12}O_{40})_2$ can be excitated by nature light.

(1) When the initial formaldehyde concentration is 69.82 mg m^{-3} at a flow rate of 40 ml min^{-1}, the amount of formaldehyde and the methanol reduce under ultraviolet light after the reaction. Methyl ether, methyl formate and formic acid are observed in the products. There are some formaldehyde but no CO_2 in the tail gas. Formic acid is the product of formaldehyde oxidation. Formic acid and methyl alcohol produce methyl formate. Part of the methanol produces methyl ether. The conversion of formaldehyde is increased according to $(NH_4)_3PW_{12}O_{40}$, $Cs_3PW_{12}O_{40}$, $Ag_3PW_{12}O_{40}$ and $Cu_3(PW_{12}O_{40})_2$, among which the catalytic effect of $Cu_3(PW_{12}O_{40})_2$ is the best and the conversion of formaldehyde over it reaches to 39.36%.
(2) When the initial formaldehyde concentration is 32.79 mg m^{-3} at a flow rate of 40 ml min^{-1}, the amount of the methanol reduces under ultraviolet light after the reaction. Methyl ether, methyl formate and formic acid are observed in the products. The formaldehyde peak vanishes in GC. There are CO_2 and no formaldehyde in the tail gas, showing that the conversion of the formaldehyde is completed. The formaldehyde is almost oxidized to formic acid, part of formic acid is further oxidized to CO_2 and H_2O.
(3) When the formaldehyde initial concentration is 14.58 mg m^{-3} (over the $(NH_4)_3PW_{12}O_{40}$ catalyst the initial concentration of formaldehyde is 5.347 mg m^{-3}) at a flow rate of 40 ml min^{-1}, the concentration of methanol reduces, but a few of methyl ether and methyl formate still appear in the exhaust gas. In the tail gas, there are no formaldehyde and formic acid, but more CO_2 is determined, showing that the formaldehyde is mainly oxidized to formic acid and most of the formic acid farther turns into CO_2 and H_2O. The remainder of the formic acid reacts with methanol to produce methyl formate. The formaldehyde is basically mineralized.

In summary, the activity of the catalysts has been found to increase in the order of $(NH_4)_3PW_{12}O_{40}$, $Cs_3PW_{12}O_{40}$, $Ag_3PW_{12}O_{40}$, $Cu_3(PW_{12}O_{40})_2$. It indicates that $M_3PW_{12}O_{40}$ catalysts increase the optical absorption and broaden the range of wavelength. The optical response of $M_3PW_{12}O_{40}$ catalysts expands into near visible light region. This is in favor of the formation of charge stream and increases the utilization of light energy. The more shift of UV–vis absorption band, the higher activity of the above catalysts is. For example, the $Cu_3(PW_{12}O_{40})_2$ catalyst has the maximal red shift to 350 nm and very strong absorption of its UV–vis absorption band, so it has some photocatalytic activity in the indoor nature light. Moreover, the particles of $Cu_3(PW_{12}O_{40})_2$ agglomerated to lower the surface energy and to form the network structure with tiny bore, which may have a better shape-selective catalysis. So the $Cu_3(PW_{12}O_{40})_2$ catalyst is identified to have the best photocatalytic activity.

4. Conclusion

Photocatalysts $M_3PW_{12}O_{40}$ ($M = NH_4^+$, Cs^+, Ag^+, Cu^{2+}) have been prepared by microwave radiation solid-phase synthesis method. SEM and XRD characterization reveals that the average particle size of $M_3PW_{12}O_{40}$ is 15–80 nm. Diffuse reflectance UV–vis spectra show that relative to $H_3PW_{12}O_{40}$, the

absorption band of $M_3PW_{12}O_{40}$ shift from 260 to 270–350 nm and the absorption band is strengthened obviously. The photocatalytic degradation of formaldehyde has been performed over $M_3PW_{12}O_{40}$. The results prove that the larger shift of UV–vis absorption band the higher activity of the catalyst is. The $Cu_3(PW_{12}O_{40})_2$ catalyst has the highest photocatalytic activity, because its red shift of UV/DRS absorption band is 90 nm and it has a network structure with a better shape-selective catalysis. The $Cu_3(PW_{12}O_{40})_2$ catalyst shows some photocatalytic activity under visible light. When the concentration of formaldehyde is 32.79 mg m^{-3}, the conversion of the formaldehyde is basically completed under the flow rate of 40 ml min^{-1} over 0.1 g $M_3PW_{12}O_{40}$ catalyst. The life of $M_3PW_{12}O_{40}$ catalysts prepared by this method is long and the catalysts can be regenerated easily. The catalysts have preferable prospective application in the photocatalytic degradation of organic contamination.

Acknowledgement

The authors gratefully acknowledge the funding of this project by Hunan Provincial Natural Science Foundation of China (05JJ30143).

References

[1] D. Sattari, C.L. Hill, J. Am. Chem. Soc. 115 (1993) 4649.
[2] C.L. Hill, D.A. Bouchard, M. Kadkhodayan, et al., J. Am. Chem. Soc. 110 (1988) 5471.
[3] B.S. Jaynes, C.L. Hill, J. Am. Chem. Soc. 117 (1995) 4704.
[4] L. Ermolenko, C. Giannotti, J. Mol. Catal. A: Chem. 114 (1996) 87.
[5] C. Tanielian, R. Seghrouchni, C. Schweitzer, J. Phys. Chem. A 107 (8) (2003) 1102.
[6] T. Yamase, E. Ishikawa, Langmuir 16 (23) (2000) 9023.
[7] T. Yamase, Chem. Rev. 98 (1998) 307.
[8] A. Mills, S. Le Hunte, J. Photochem. Photobiol. A 108 (1997) 1.
[9] P.V. Kamat, Chem. Rev. 93 (1993) 267.
[10] H. Hidaka, S. Horikoshi, K. Ajiaka, et al., J. Photochem. Photobiol. A: Chem. 108 (1997) 197.
[11] D.A. Friesen, L. Morello, J.V. Headley, et al., J. Photochem. Photobiol. A: Chem. 133 (2000) 213.
[12] Y. Guo, C. Hu, S. Jiang, et al., Appl. Catal. B: Environ. 36 (2002) 9.
[13] A. Mylonas, A. Hiskia, E. Papaconstantinou, J. Mol. Catal. A: Chem. 114 (1996) 19l.
[14] D. Li, Y. Guo, C. Hu, et al., Appl. Catal. A: Gen. 235 (2002) 11.
[15] A. Idil, J.L. Ferry, Dyes Pigments 54 (2002) 25.
[16] B. Bai, J. Zhao, X. Feng, Mater. Lett. 57 (2003) 3914.
[17] C. Jiang, Y. Guo, C. Hu, et al., Mater. Res. Bull. 39 (2004) 251.
[18] Y. Yang, Y. Guo, C. Hu, et al., Appl. Catal. A: Gen. 252 (2003) 305.
[19] S. Anandan, S.Y. Ryu, W. Cho, et al., J. Mol. Catal. A: Chem. 195 (2003) 201.
[20] Y. Yang, Q. Wu, Y. Guo, et al., J. Mol. Catal. A: Chem. 225 (2005) 203.
[21] L. Li, Q. Wu, Y. Guo, et al., Micropor. Mesopor. Mater. 87 (2005) 1.
[22] Y. Yang, Y. Guo, C. Hu, et al., Appl. Catal. A: Gen. 73 (2004) 201.
[23] K. Zhang, W. Cao, J. Zhang, Appl. Catal. A: Gen. 276 (2004) 67.
[24] W. You, Y. Wang, E. Wang, et al., Chem. J. Chin. Univ. 21 (2000) 1636.
[25] G. Pang, D. Cui, W. Xu, et al., Acta Chim. Sin. (Huaxue Xuebao) 54 (1996) 757.
[26] L. Zhou, S. Liu, G. Yu, et al., Chin. J. Chem. Phys. 16 (2003) 411.
[27] E. Wang, C. Hu, L. Xu, Introduction of Heteropoly Chemistry, Chemical Industry Press, Beijing, 1998, p. 4.
[28] C. Hu, E. Wang, L. Xu, Chin. Sci. Bull. 42 (1998) 1234.
[29] K.C. ckiewicz, G. Zúukowska, W. Wieczorek, Chem. Mater. 13 (2001) 379.
[30] C. Cheng, Y. Su, Chin. J. Inorg. Chem. 7 (1991) 208.